

## COMPLEX TRIGLYCINE SULPHATE (TGS) CRYSTAL ANALYSIS

Horia V. ALEXANDRU<sup>16</sup>

Reception speech at the Academy of Scientists,  
January 26, 2023

DOI <https://doi.org/10.56082/annalsarscipphyschem.2023.1.93>

It is with emotion that I deliver before you the traditional speech of reception, on which occasion my thoughts turn to all those who, over more than five decades, have shared with me, in one way or another, the same concerns in researching experimental and theoretical aspects of crystal growth or its applications.

Certainly, the progress of modern society would not have been the same without the science of crystal growth. Most semiconductor devices today are made from single crystals, with research in the field often pointing out that the advent of semiconductor devices was always preceded by the invention of new crystal growth technologies. Over time, considerable efforts have been made to clarify the static characteristics of the surfaces and the quality of the crystals, using various sophisticated tools such as X-ray diffraction, electron microscopy or scanning microscopy. On the other hand, the studies also considered the dynamic behavior of atoms and molecules on the surface of a growing crystal. Therefore, tools such as thermodynamics, statistical physics, and quantum mechanics must be used to understand the mechanism of crystal growth, along with up-to-date notions of crystallography.

Over the years, a constant of my crystal growing research has been directed towards the Triglycine Sulfate crystal, to which I wish to draw your attention in what follows. This is an important ferroelectric crystal used across a wide spectrum of radiation detection.

The ferroelectric crystal Triglycine Sulfate (TGS) presents distinct properties in the ferroelectric phase on the four temperature ranges  $T_c$ -45-40-35-30-(25)°C, for all measurement parameters [1]. The lower limit of the ferroelectric transition was set by us at 28-30°C, about 20°C below The Curie point (49.2 °C). The crystals

---

<sup>16</sup> Academy of Romanian Scientists

grown by slow evaporation of the solvent, in the paraelectric phase, were cleaved, polished and silver paste electrodes were deposited.

The TGS substance, purified by fractional recrystallization, measurements of growth kinetics and the influence of impurities have been presented by us in the literature. A special three-step method was used, by drawing a first fraction from the solution (about 10%), to remove impurities with a  $CS/CL > 1$  coefficient. The parent material, previously purified by fractional recrystallization, was used to grow pure TGS crystals in the para phase at 54°C by slow solvent evaporation.

An Alpha-A Novocontrol dielectric spectrometer was used to create the temperature program (see fig.1) and to record the real and imaginary components of epsilon. The measurements were performed with a temperature program 65 / -120°C, passing down (Z2 and Z5) and up (Z3) through the Curie point at 0.6°C/minute. A.C. conductivity was evaluated from the  $\epsilon''$  component with the help of the program installed on the spectrometer's computer, for the entire frequency spectrum.

Five equidistant points were measured in each frequency range (1 to 107 Hz) in continuous mode for one set of meters, passing up and down the Curie point (fig.1).

The imaginary component of the permittivity, as a function of frequency, is shown in fig.2 at 46 °C. Conduction losses (blue line in fig.2) decrease linearly with frequency and have significantly higher values at low frequencies.

The absolute and relative values of the conduction components, at the representative frequencies 1 Hz, 1 KHz, 1 MHz are presented in fig.2, the red component representing  $\epsilon''$ , without conduction losses.

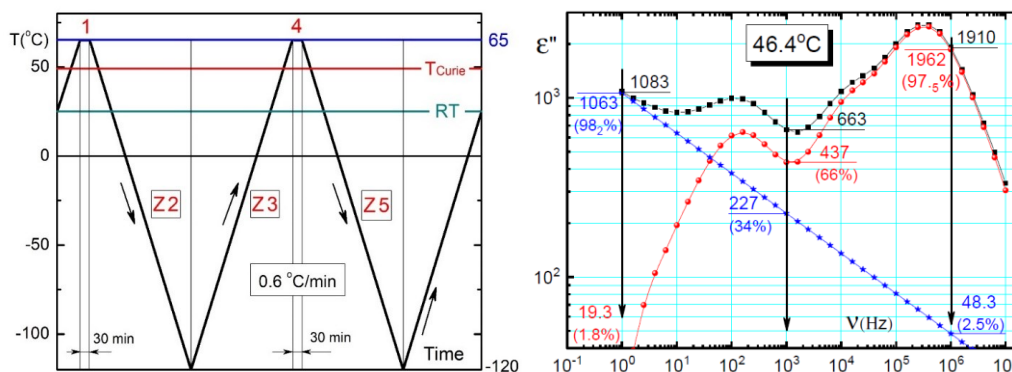


Fig.1 [1]

Fig.2 [1]

In fig. 3 are presented, for zones Z2 and Z3, conductive losses of the permittivity, depending on the frequency at different temperatures. At frequencies of 4 - 6 Hz the Z2 lines have a congruent point. The Z3 curve (as the temperature increases) shows a disorder between 45°C and Tc. Below the temperature of 45°C the components decrease monotonically until 25 °C, where the transition appears as finished, because to zero Celsius follows an empty space.

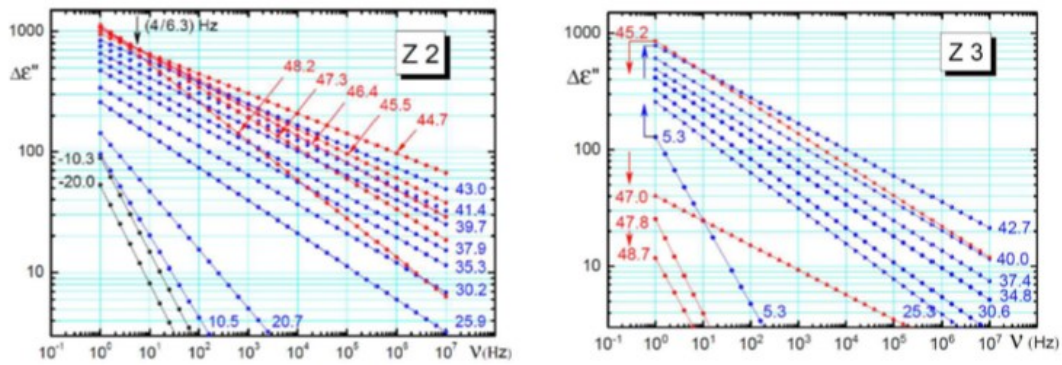


Fig. 3. The evolution of permittivity (loss comp.) with frequency for Z2, Z3 [1].

**In zone Z3, a strong disturbance is observed in the Tc-45°C temperature range.** Below 45 °C the curves look similar. Curves Z2 and Z5 have a congruent point at 4-6 Hz [1]

The evolution of the permittivity loss components is shown in fig.3 for Z2/Z3.

For zone Z5, the curves are similar to those in zone Z2. It should be noted that at frequencies, of the order of 10 MHz, on the same temperature range, the conductivity loss components have considerably lower values by 1 or 2 orders of magnitude.

The equations of the Debye components, which consider a unique relaxation time and include a conduction term (in eq.2) are :

$$\varepsilon' = \varepsilon_{\infty} + \frac{\Delta\varepsilon}{1 + \omega^2\tau_{\varepsilon}^2} \quad (1) \quad \varepsilon'' = \frac{\omega\tau_{\varepsilon}(\Delta\varepsilon)}{1 + \omega^2\tau_{\varepsilon}^2} + \frac{\sigma}{\varepsilon_0\omega} \quad (2)$$

where  $\varepsilon_{\infty}$  is the dielectric constant at high frequencies,  $\Delta\varepsilon = \varepsilon_{st} - \varepsilon_{\infty}$  is the difference between the extreme values of permittivity, and the second term in equation (2) represents conduction losses.

**Conductivity and permittivity are related by the equation :**

$$\sigma^*(\omega) = \sigma' + j \sigma'' = j \omega \varepsilon_0 \varepsilon^*(\omega) = j \varepsilon_0 \omega [\varepsilon' - j \varepsilon''] = \omega \varepsilon_0 \varepsilon'' + j \omega \varepsilon_0 \varepsilon' \quad (3)$$

**The first term in equation (3), at low frequencies of the order of 1 Hz (or lower), becomes dominant and represents conduction losses in the material.**

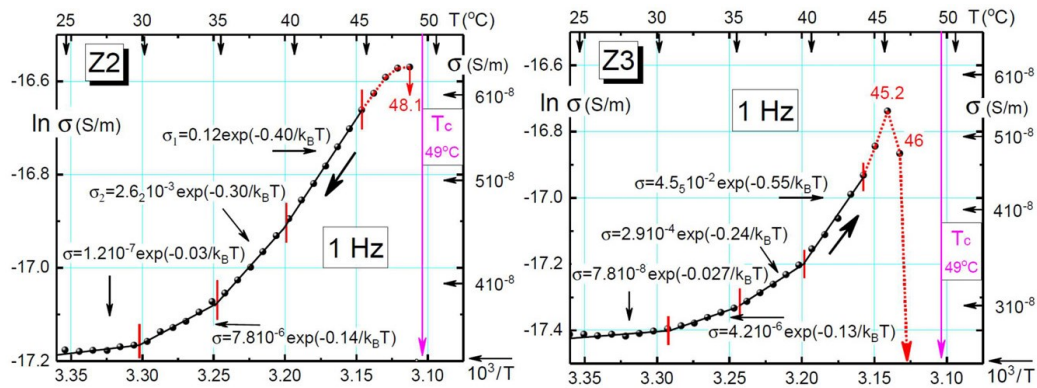
In fig. 4 shows the conduction in Arrhenius coordinates for Z2 and Z3, estimated from equation (3), with the help of permittivity data.

The conduction activation energy was estimated from the equation :

$$\sigma = \sigma_0 \exp(-\Delta E / K_B T) \quad (4)$$

and is shown in fig.4 on different temperature zones.

**In the temperature range 25°C and 30°C**, the activation energy, deduced from equation (3) is of the **order of  $K_B T$  (0.026 eV)** and indicates that the lower limit of the transition in TGS is close to 30°C, in agreement with Slosarek's data (29°C), specified in the journal Phys. State. Sol. (b) 110 (1982) 233, [2], [8]



[1] Fig.4 Conductivity in Arrhenius coordinates, for areas Z2, Z3.

The activation energies can be seen in the equations for sigma in fig 4.

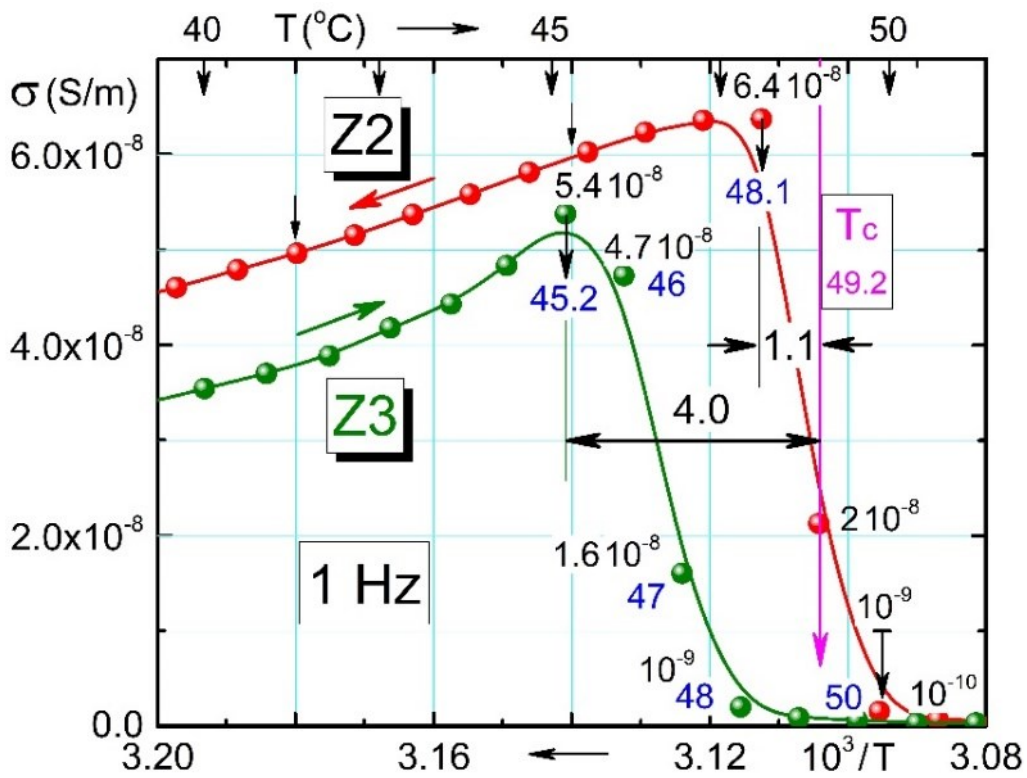
In this figure, on the temperature range 45°C - $T_c$ , important disturbances can be observed for Z2 and Z3. In this temperature range, the system is not stable and internal changes occur, probably in the walls of the ferroelectric domains, sensitive to the temperature variation.

The decrease in the value of the activation energy with decreasing temperature, below the Curie point, indicates that the domain walls are involved. The conductivity of zone Z3 when the temperature increases, decreases compared to that of zone Z2 (when the temperature decreases) and is much shifted towards

much lower values, approximately 4°C compared to the transition temperature  $T_c=49.2^\circ\text{C}$ .

Table 1. Conductivity activation energy in equation (4), by temperature zones [1]

	Temp. ( $^\circ\text{C}$ )	45 ÷ 40	40 ÷ 35	35 ÷ 30	30 ÷ 25
Z2	$\Delta E$ (eV)	0.40	0.30	0.14	0.03
Z3	$\Delta E$ (eV)	0.55	0.24	0.13	0.027
Z5	$\Delta E$ (eV)	0.36	0.29	0.15	0.03



**Original** - Fig.5. The maxima of the conduction  $\sigma$ , for the curves Z2 and Z3 are separated in the ferro phase by 1°C and 4°C, compared to the transition temperature  $T_c=49.2^\circ\text{C}$ .

The Cole-Cole equations for the permittivity components are:

$$\epsilon' = \epsilon_{\infty} + (\epsilon_{st} - \epsilon_{\infty}) / (1 + \omega^2 \tau^2)^{1-N} \quad (5)$$

$$\epsilon'' = \omega \tau (\epsilon_{st} - \epsilon_{\infty}) / (1 + \omega^2 \tau^2)^{1-N} + (\sigma / \epsilon_0 \omega)^N \quad (6)$$

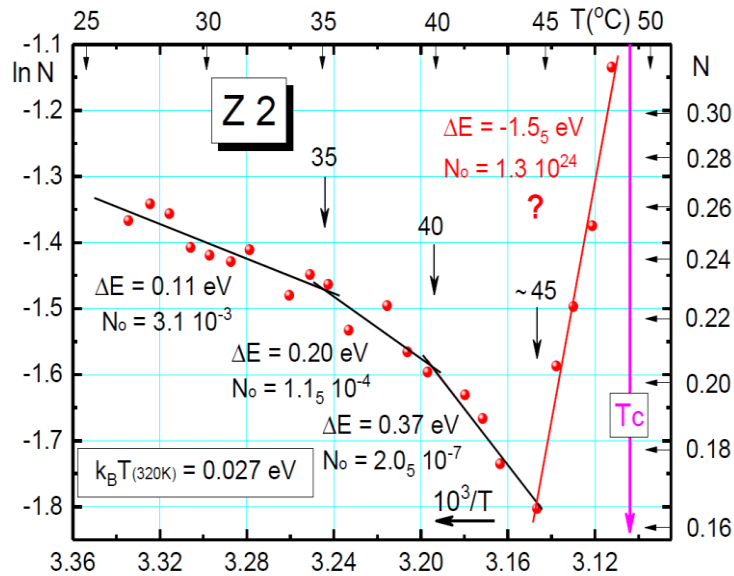
where  $(\epsilon_{st} - \epsilon_{\infty}) = \Delta\epsilon$  represents the difference between the extreme values of the permittivity, and  $N$  is the Cole-Cole coefficient that takes into account the fact that the center of the Debye circle is lowered below the X-axis.

The conduction component of the term  $\epsilon''$ , estimated by the computer, from equation (2), as a function of frequency, at 46.4°C, was represented in fig. 2. The term does not correspond to the Cole-Cole equations :

$(\sigma / \epsilon_0 \omega)^N$ , but dependence is found experimentally  $\log \sigma \sim N \log \omega$ .

### Component N from equations (5) and (6)

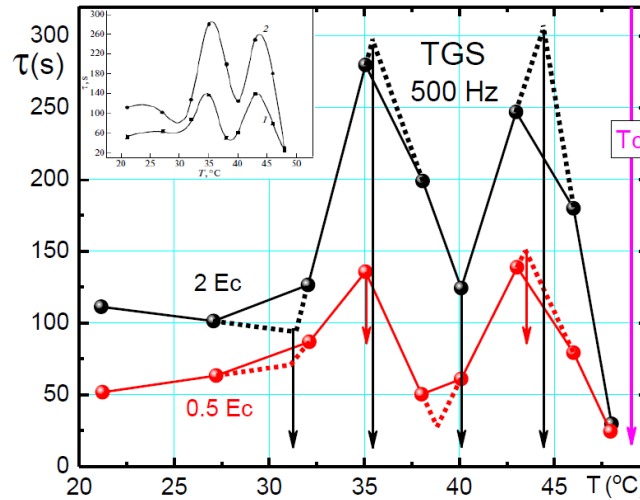
It has an Arrhenius behavior with temperature, in the ferroelectric phase, as shown in fig. 6. The coefficient  $N$  has different activation energy values between 25°C and 45°C, decreasing by 0.11 / 0.20 / 0.37 eV on the three temperature ranges. At 45°C, inexplicably, the slope suddenly changes and increases from 0.16 to 0.34 in this area, which can be seen in fig 6 and in table 2.



[1] - Fig. 6. Activation energy for the coefficient  $N$  over the temperature range 25°C and  $T_c$

[1] Table 2. Arrhenius parameters of the N coefficient in the Z2 area, eq. (7) and fig.5.

Temp. (°C)	$T_c \div 45$	45 - 40	40 - 35	35 - 25
$\Delta E_N$ (eV)	-1.55 (?)	0.37	0.20	0.11
$N_0$	$1.3 \cdot 10^{24}$ (?)	$2.0_5 \cdot 10^{-7}$	$1.1_5 \cdot 10^{-4}$	$3.1 \cdot 10^{-3}$



[1] - Fig.7. The temperature dependence of the relaxation times of  $\epsilon'$  (in seconds) for TGS. The applied field is 0.5  $E_c$  and 2  $E_c$  at the a frequency of 500 Hz (where  $E_c$  is the coercive field).

Data were reviewed by us after O.M.Golitsyna, S.N.Drozhdin, Pys. of Solid State, **53** (2011) 341.

This evolution appears to be related to the structure and evolution of the ferroelectric domain walls in the TGS crystal - C. Mîndru et al, JOAM 14 (2012) 157 – [11]

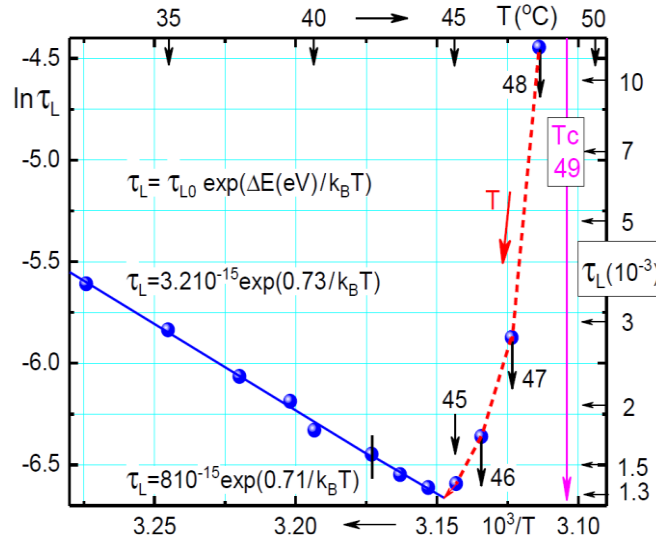
Considering  $d\epsilon(t)/dt$ , the rate of relaxation of the permittivity proportional to the distance to the equilibrium position  $[\epsilon(t) - \epsilon_\infty]$ , at any moment (as in the case of elastic forces), we have:

$$d\epsilon(t)/dt = (\epsilon(t) - \epsilon_\infty) / \tau \quad (7)$$

where the relaxation time  $\tau$  was calculated by integration, using the experimental data shown in fig. 7:

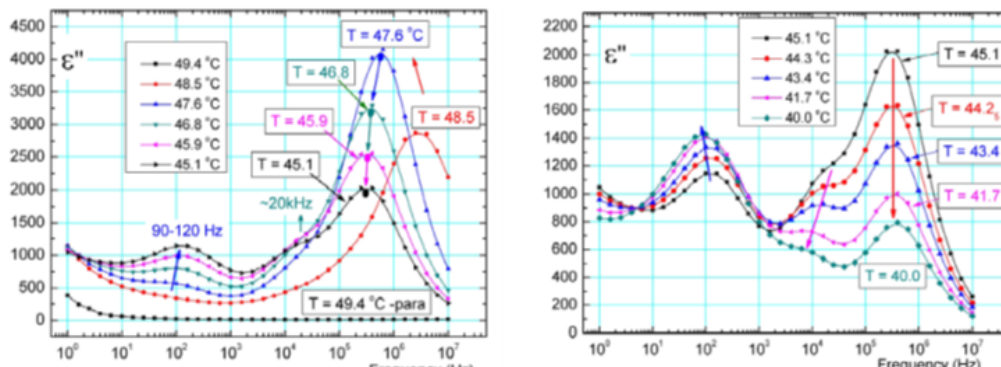
$$\epsilon(t) - \epsilon_\infty = (\epsilon|_{t=0} - \epsilon_\infty) \exp(-t/\tau) \quad (8)$$

We estimated (red curve in Fig. 7) the permittivity relaxation times,  $\tau_1 \approx 130$  sec. at 35°C and  $\tau_2 \approx 150$  sec at 43°C, for the applied field of 0.5 Ec (coercive field), at 500 HZ.



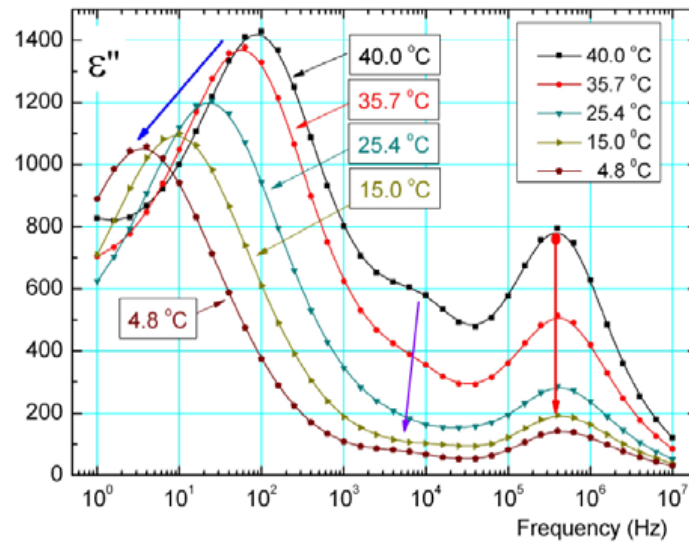
[1] - Fig. 8. Relaxation time for TGS (in sec.) at low frequencies, in Arrhenius coordinates.

**The relaxation time  $\tau_L$** , around the temperature of 45°C, has a turning point, like the coefficient N in the Arrhenius scale (figs.6 and 8). In the Cole-Cole representations of the  $\epsilon''$  diagrams there are three relaxations with frequencies of: up LOW ( $10^2 \div 10^3$  Hz), down for High ( $10^5 \div 10^6$  Hz) and MIDDLE ( $\sim 10^4$  Hz). **In the 45°C-Tc area, they have a non-Arrhenius dependence, probably**



[4] - Fig. 9. Temperature dependence between Tc – (45—40) °C of the three components of  $\epsilon''$ , over the entire measured frequency range. The HIGH and MIDDLE curves have maxima at  $5 \cdot 10^5$  Hz and  $\sim 10^4$  Hz, decreasing with temperature, while the LOW curve, with a maximum around  $10^2$  Hz increases continuously.

indicating that other types of forces act here.

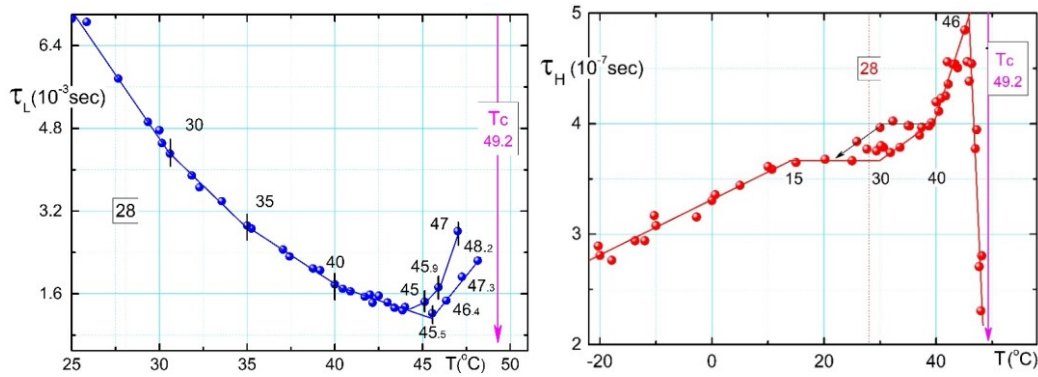


[4]. Fig. 10. Below the temperature of 40°C the HIGH and MIDDLE components further decrease, while the LOW component (blue line) drops and moves to lower frequencies.

### Relaxation times and their activation energies

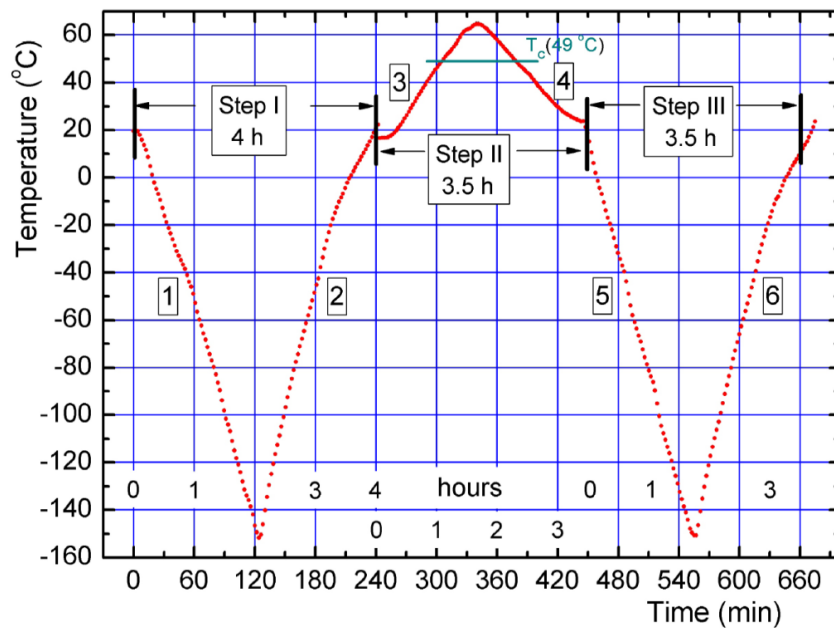
Their values were calculated from the  $\tau \omega = 1$  i.e.  $\tau = 1 / \omega = 1 / 2\pi \nu$

The relaxation times for the LOW and HIGH curves were found to have opposite directions of variation with temperature. Above 45°C,  $\tau_L$  (of the order of  $10^{-3}$  sec.) increases and appears to have two types of values, while  $\tau_H$  (of the order of  $10^{-7}$  sec.) decreases towards the transition temperature  $T_c$ .



**ORIGINAL** - Fig. 11. The relaxation time for the LOW and HIGH curves depending on the temperature.

The relaxation times for the LOW and HIGH curves were found to have opposite directions of variation with temperature. Above  $45^{\circ}\text{C}$ ,  $\tau_L$  (of the order  $10^{-3}$  sec.) increases and appears to have two types of values, while  $\tau_H$  (of the order of  $10^{-7}$  sec.) decreases towards the transition temperature.



[24]. Fig.12. Measurements of temperature-time dielectric parameters in 6 temperature steps.

As seen in fig. 12, measurements were made in three steps at 300 Hz.

The measurements on routes 3, 4, 5, 6 are presented in detail in fig. 13. They have an absolute minimum around the temperature of approximately  $-56^{\circ}\text{C}$ , according to the specifications: G. Slosarek et al, Phys. State. Soil. (b) 110 (1982)

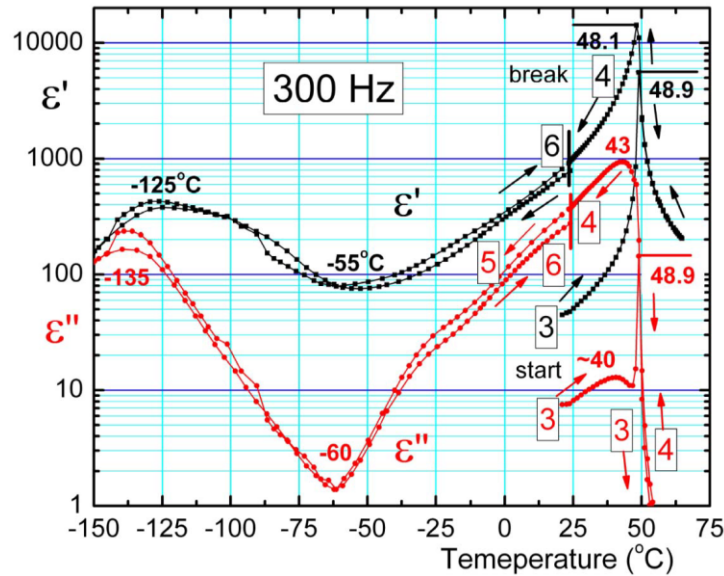


Fig.13. The temperature dependence of the two components of the permittivity, at the frequency of 300 Hz, along routes 3, 4, 5 and 6 in fig.1. Routes 1 and 2 with low permittivity values, were omitted – [24]

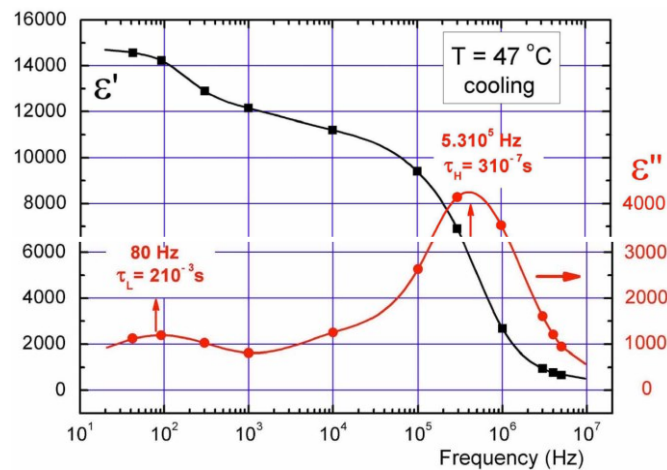


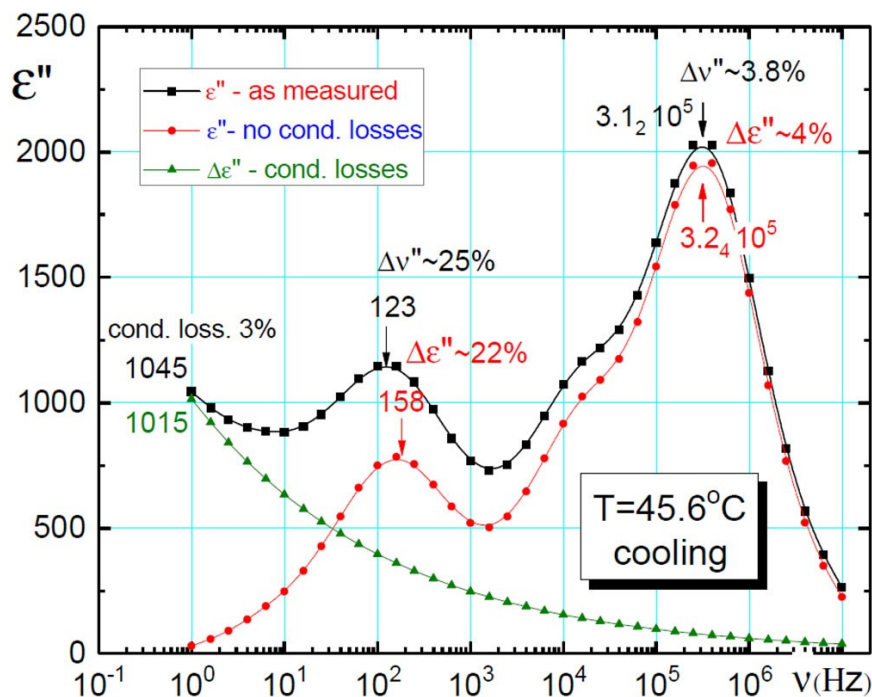
Fig.14. Frequency dependence of permittivity components at  $47^{\circ}\text{C}$ .

Two relaxation mechanisms are observed LOW at  $\sim 10^2$  Hz and 0.5 MHz

The MIDDLE component, less highlighted, stands out at  $10^4$  Hz – [24]

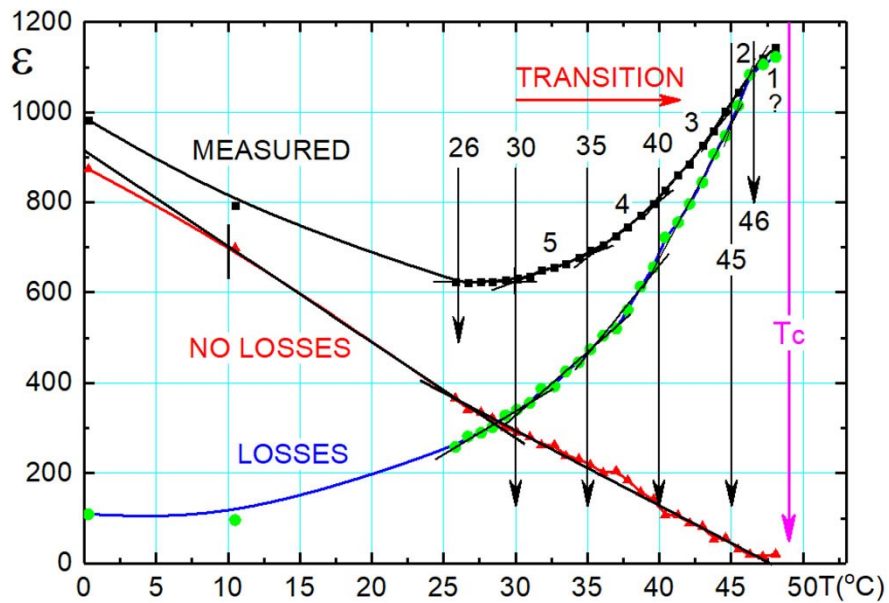
In Fig. 13 the two components of the permittivity highlight the transition from  $49.2^\circ\text{C}$ , the transient values and the absolute minimum at  $-56^\circ\text{C}$ , anticipated by Slosarek ref.[2]. Each frequency has its own path, but all have the same landmarks. In fig.14, two important components of the dielectric constant of the TGS near the transition are highlighted. They have different intensities, have a specific course, their evolution being characteristic of each component.

**Dielectric Spectroscopy of TGS**, H.V.Alexandru, *Ferroelectrics* **558** (2020) 36 – [6]

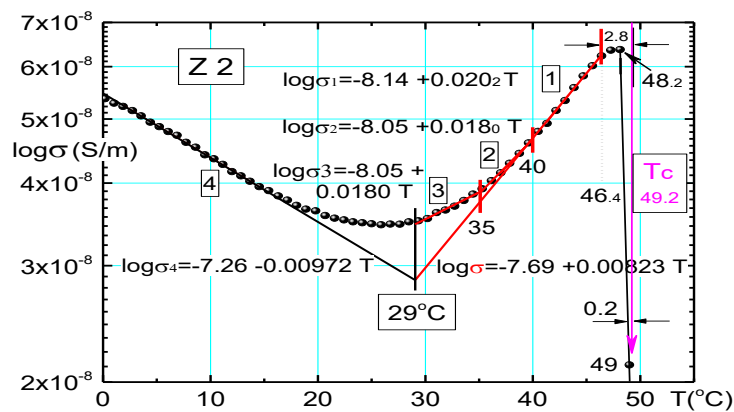


[6].Fig. 15. The two active components in TGS at  $45^\circ\text{C}$ . The red component at  $158\text{Hz}$  is shifted from the measured one, as is the high frequency component at  $3.2 \cdot 10^5 \text{ Hz}$

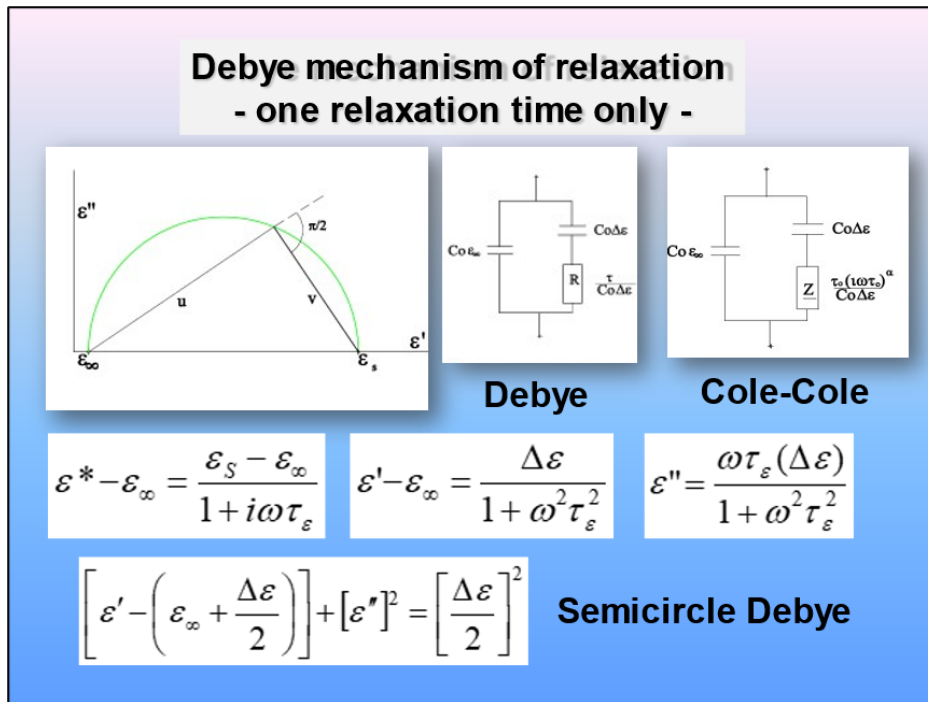
The maxima that appear in figure 15 are: 1/ the maximum of the curve at  $5.5\text{MHz}$ , which corresponds to Group G1 in TGS, 2/ the maximum at  $10^4 \text{ Hz}$  corresponds to the hydrogen bridge G2-G3; both decrease with decreasing temperature, and the one at  $1\text{Hz}$  is active, continuing to increase with decreasing temperature.



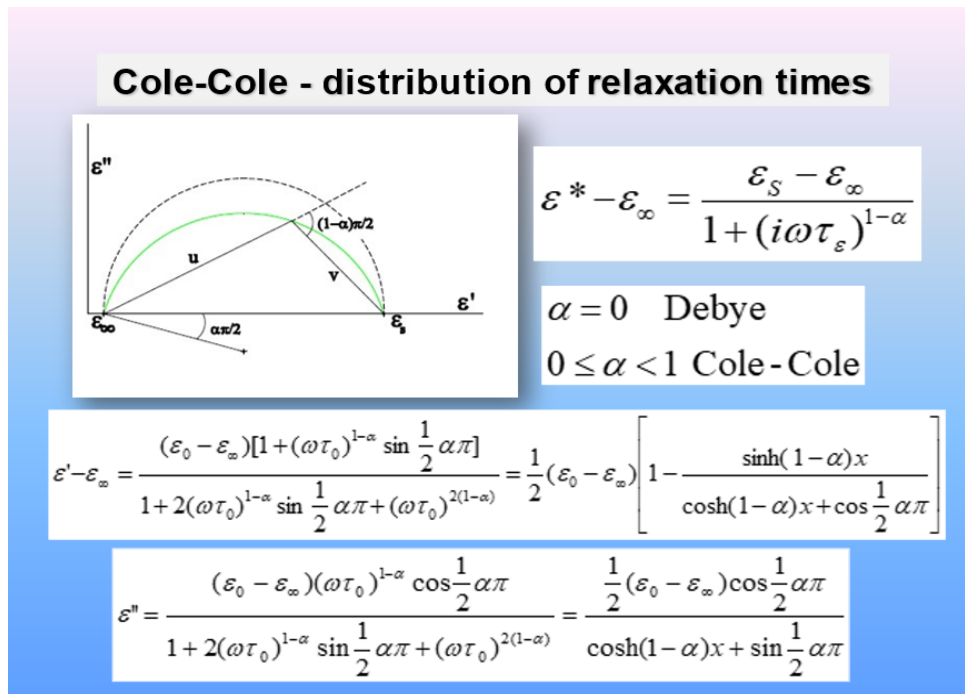
[6] Fig. 16. Zones in the ferroelectric transition of TGS. It is observed that the lowest value is around 29°C, where the measured curve has a minimum. The loss curve is similar to that of the measured values. The dielectric constant curve measured without losses decreases linearly in zone 29



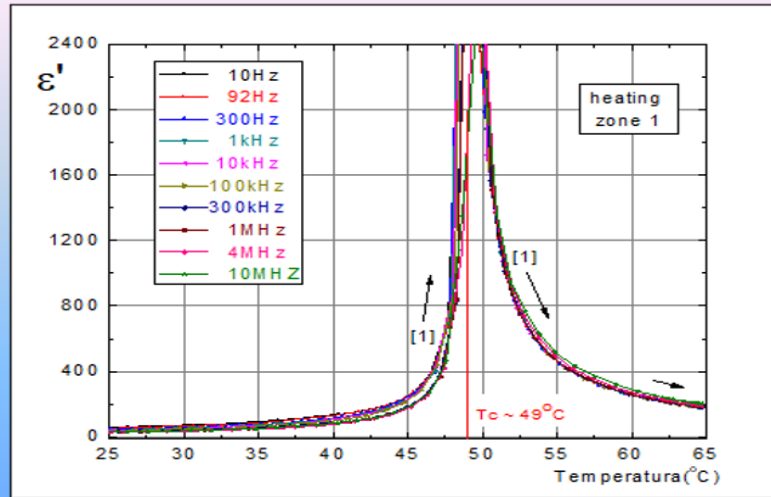
[6] Fig. 17. The conductivity as a function of temperature indicates that at 29°C there is a change in slope, which marks the transition to another working regime.



ORIGINAL - Fig. 18 Debye semicircle and equivalent scheme

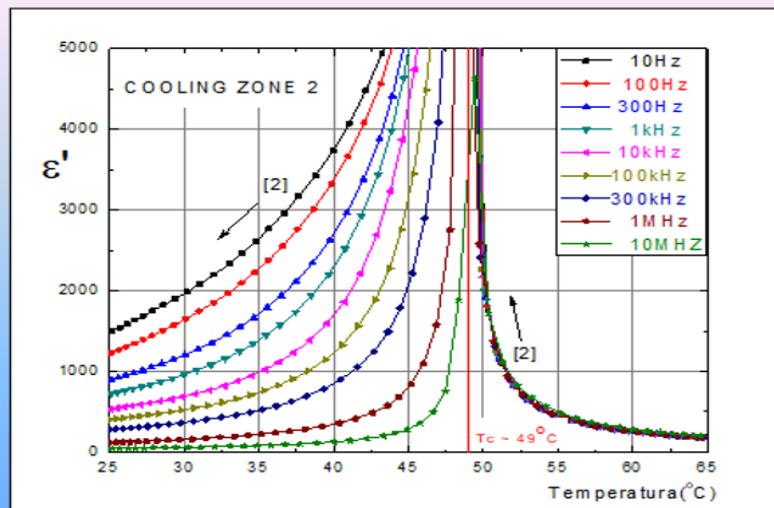


ORIGINAL - Fig. 19 Cole-Cole spring and equivalent scheme



**No dispersion on heating through the Curie Point after several weeks of relaxation or for virgin samples**

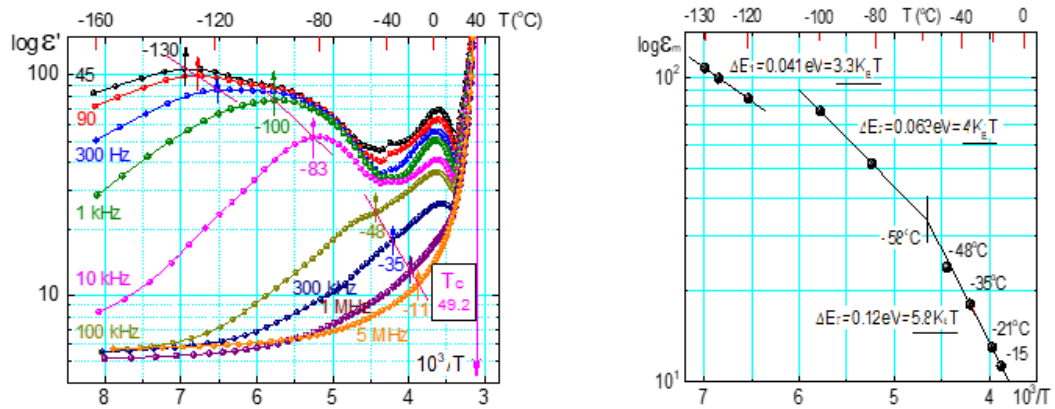
ORIGINAL – Fig. 20 The permittivity at the increase the temperature



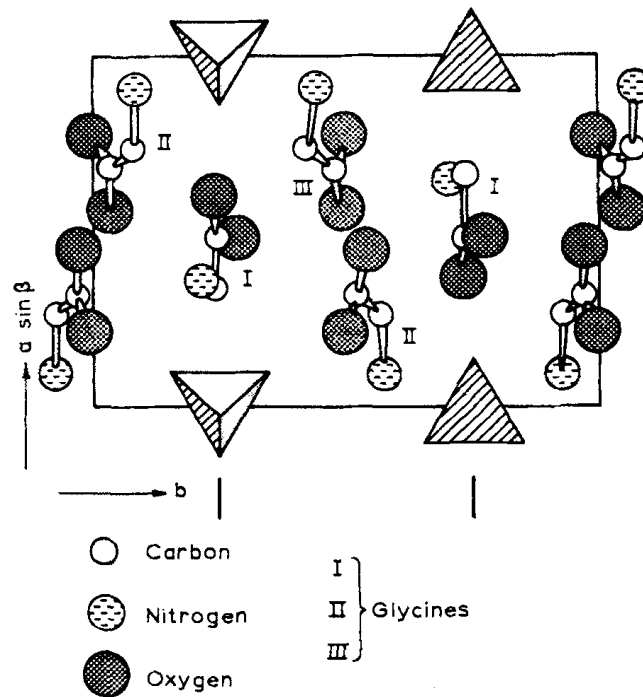
**Large dispersion on cooling through the Curie Point and no dispersion in paraelectric phase**

ORIGINAL – Fig.21 Permittivity when the temperature drops

At low negative temperatures, a dispersion of transition points occurs. In Arrhenius coordinates they are placed in three groups below 0°C. In the figure on the right, in the Arrhenius scale, the three lines are represented, together with their activation energies. Two of them meet at -56°C.



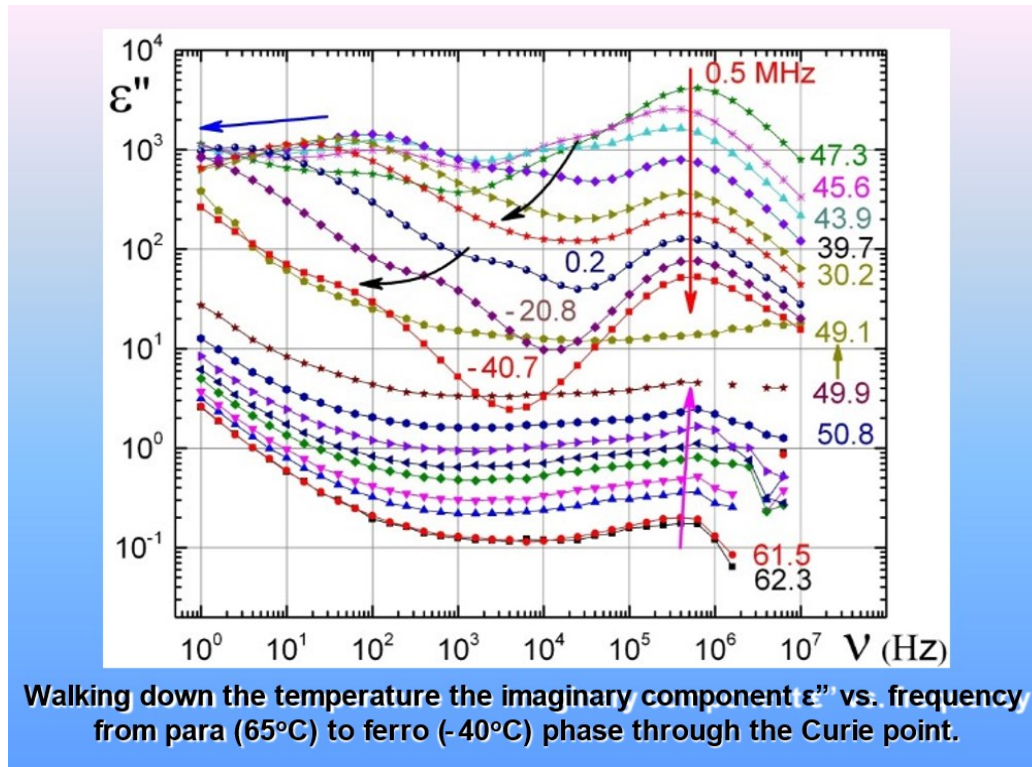
**ORIGINAL - Fig. 22.** Left - The three straight ones (marked in red) below zero Celsius and Right - Their activation energies in Arrhenius coordinates.



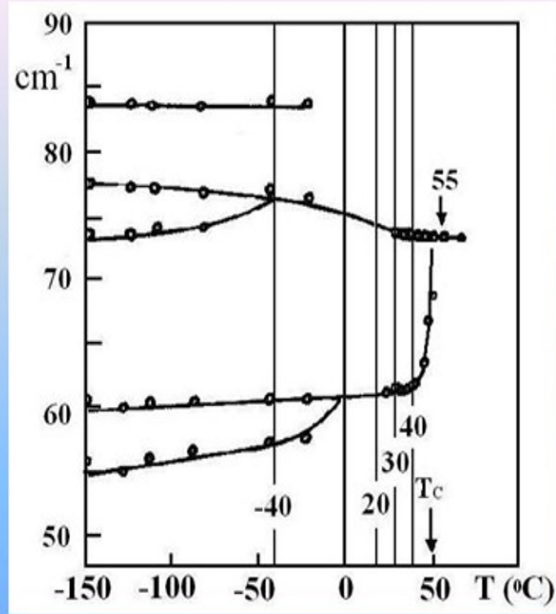
[25] Fig. 23. E. T. Keve et al *Ferroelectrics* vol 3 (1971) 39-48  
TGS structure along the X-axis

In Fig 23 there are two TGS groups in the Structure. You can see the GI groups in the center and the GII - GIII groups connected by a hydrogen bridge.

Sulfate groups are represented by tetrahedra. The Glycine I group has two symmetrical positions with respect to the m-planes and switches to inversion of polarization.



**ORIGINAL** - Fig. 24. The imaginary component of the permittivity  $\epsilon''$  as a function of the frequency in the para over phase (62.5°C) and below the transition temperature  $T_c=49.2^\circ\text{C}$ .

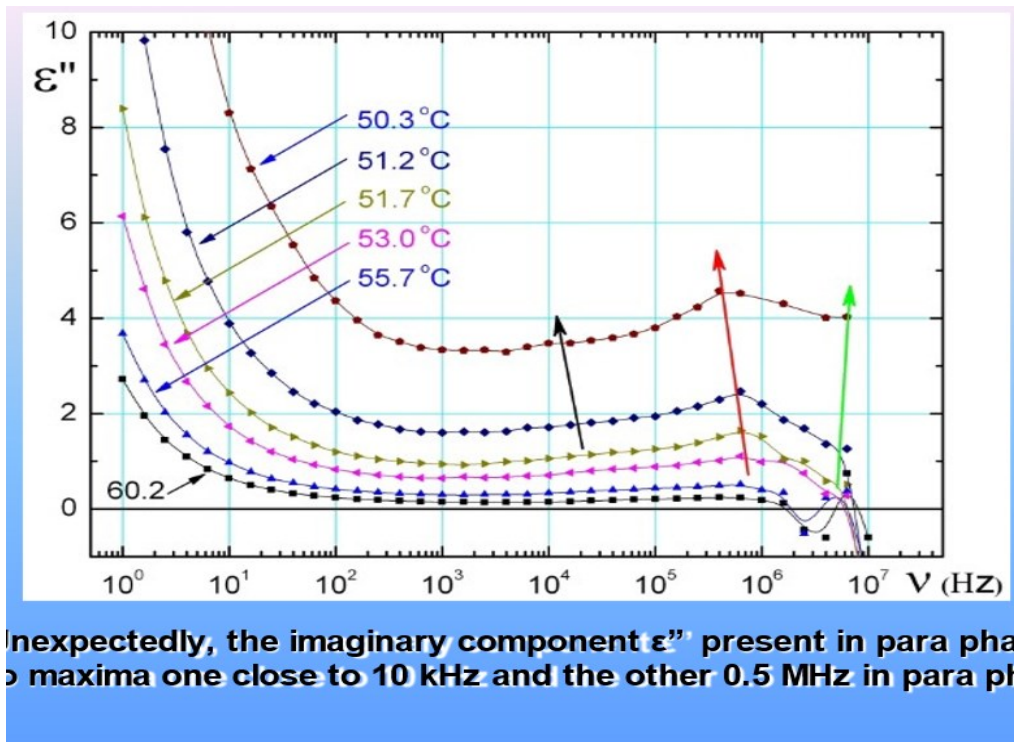


The temperature dependence of Raman external mode in TGS.

We have redrawn this graphic using the data from:

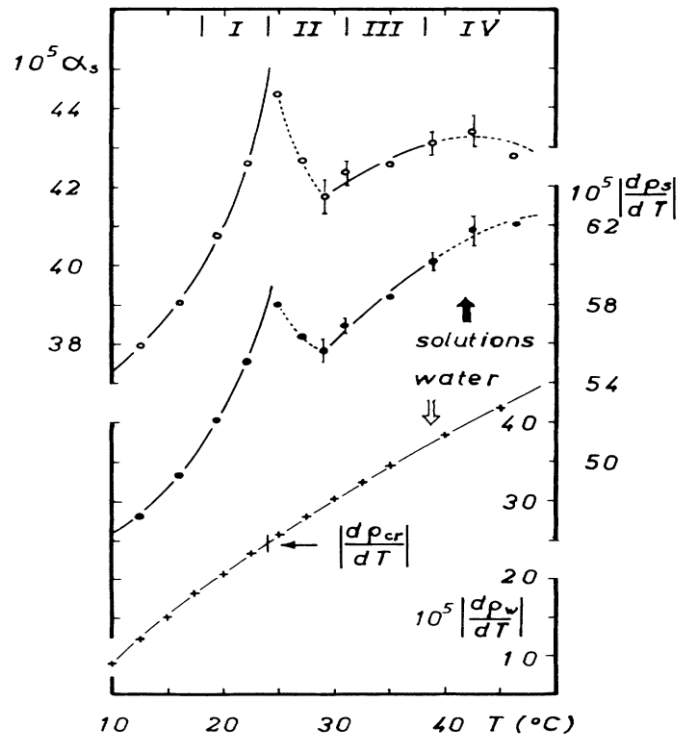
**P.O.Cervenka et al, *Ferroelectrics* 11 (1976) 511**

[7] Fig.25.



**ORIGINAL** Fig. 26. In para phase, between transition temperature  $T_c$  and  $54^\circ\text{C}$  in para phase, still appears two maxima at 0.5 MHz and approximately 104 Hz

Although not related to the topic chosen for my acceptance speech, I still want to submit to your attention an achievement, it seems unique in the literature: the influence of the transition of the **solute in the Rochelle salt solution**, studying its density and dielectric capacity.



[26] Fig. 27.

Top: Variation with temperature of the coefficient of volume expansion as unction of temperature for the saturated Rochelle Salt solution, at 24°C. Bottom: Same curve for regular distilled water on the same temperature range.

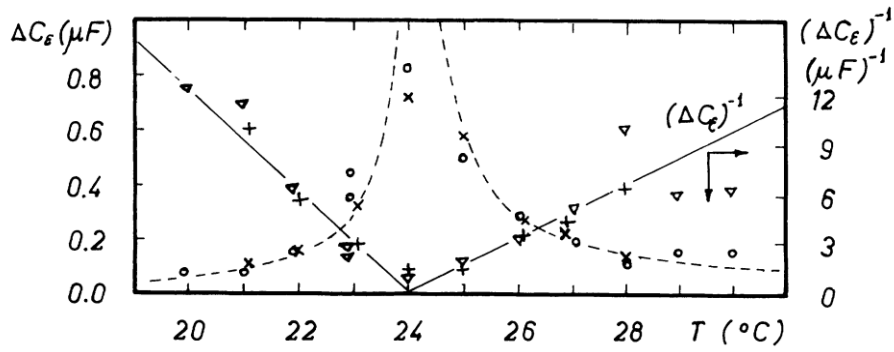


Fig. 28. The ferroelectric components of the Rochelle Salt solution, saturated at 24°C and its inverse as a function of temperature— [26]

## R E F E R E N C E S

- [1.] **H. V. Alexandru**, Stages in Ferroelectric Transition of TGS. *Ferroelectrics* **551** (2019) 211-228).
- [2.] G. Slosarek et al., Anisotropy of the relaxation time  $T_1$  of  $\text{NH}_3$  groups in triglycine sulphate crystals, *Phys. Stat. Sol. (B)* **110** (1982) 233.
- [3.] D. Marinel, **H. V. Alexandru**, C. P. Ganea, Conductivity losses in ferroelectric phase of TGS *J. Optoelectronics Adv. Materials* **20** (2018) 676-681
- [4.] C. Mindru, C. P. Ganea, **H. V. Alexandru**, Dielectric relaxation of pure TGS crystals *J. Optoelectr. Adv. Materials* **14** (2012) 157-162
- [5.] **H. V. Alexandru**, D. Marinel, C. Mindru, C. Ganea, Parameters in Ferroelectric Phase of TGS, *Ferroelectrics*, **583** (2021) 106-124
- [6.] **Horia V. Alexandru**, Dielectric spectroscopy of TGS, *Ferroelectrics* **558** (2020) 36-45,
- [7.] P. O. Cervenka et al., The ferroelectric phase transition and dielectric anomaly in triglycine sulfate, *Ferroelectrics*. **11** (1976) 511
- [8.] G. Slosarek et al., A study of the paraelectric-ferroelectric phase transition of TGS by deuteron nuclear magnetic resonance and relaxation, *J. Phys. Condens. Matter.* **1** (1989) 5931.
- [9.] C. P. Ganea, C. Mindrub, N. Vineticu, **H.V. Alexandru** Dielectric spectroscopy in paraferro transition of TGS, *Ferroelectrics* **493** (2016) 165
- [10.] **H. V. Alexandru**, and C. Mindru, Temperature dependence of Cole-Cole and dielectric strength parameters of TGS crystal, *Ferroelectrics*. **505** (2016) 216
- [11.] C. Mindru, C. P. Ganea, and **H. V. Alexandru**, Dielectric relaxation of pure TGS crystals, *J. Optoelectr. Adv. Mater.* **14** (2012) 157
- [12.] J. Zang, Dielectric dispersion of domain wall motion of triglycine sulfate, *Phys. Stat. Sol. (a)*. **193** (2002) 347.
- [13.] J. Zang, Dynamical property of domain walls of triglycine sulfate in the vicinity of  $T_c$ , *Ferroelectrics*. **281** (2002). 105
- [14.] **H. V. Alexandru** et al., Growth and kinetic measurements of triglycine sulphate crystals, *Cryst. Res. Technol.* **30** (1995) 307
- [15.] **H. V. Alexandru**, Segregation of impurities in crystal growth from solutions, *J Optoelectr. Adv. Mater.* **9** (2007) 1227
- [16.] **H. V. Alexandru**, Pure and doped TGS crystals, *Ann. N. Y Acad. Sci.* **1161** (2009) 387.
- [17.] **D. Marinel**, **H. V. Alexandru**, C. P. Ganea, Conductivity losses in ferroelectric phase of TGS, *J Optoelectr. Adv. Mater.* **20** (2018) 676
- [18.] O. M. Golitsyna, S. N. Drozhdin, Relaxation stimulated in the domain structure of a TGS crystal by an alternating-current electric field, *Phys. Solid State.* **53** (2011) 341

- 
- [19.] **H. V. Alexandru**, Second-order transition in Rochelle-salt saturated solutions, Phys. Rev.A. **45** (1992) 8632
- [20.] **H.V. Alexandru**, C. Berbecaru, F. Stanculescu, Doped TGS crystals for IR detection and sensors, Sensors and Actuators A **113** (2004) 387–392
- [21.] **Horia V. Alexandru**, Dielectric spectroscopy of TGS, Ferroelectrics **558** (2020) 36–45
- [22.] **H. V. Alexandru**, M. Dan, C. Ganea, TGS dynamics in relation with temperature and Bias field Annals of the Academy of Romanian Scientists on Physics and Chemistry **6** (2021) 29
- [23.] **H. V. Alexandru**, C. Mindru, R. Bacsei, C.-P. Ganea, Estimation of essential dielectric parameters in ferroelectric state of TGS crystal, J. Opto. Adv. Materials **16** (2014) 457
- [24.] **H. V. Alexandru**, C. Mindru, C. Berbecaru, Dielectric relaxation of TGS crystal in the second order phase transition. Digest J. Nanomaterials and Biostructures **7** (2012) 1353 – 1364
- [25.] E. T. Keve, K. L. Bye, P. W. Whiipps A. D. Annis, Structural Inhibition of ferroelectric switching in TGS- I. admixtures, Ferroelectrics, **3** (1971) 39-48
- [26.] **Horia V. Alexandru**, “Second order transition in Rochelle Salt saturated solutions” Physical Review A **45** (1992) 12